Journal of Peptide Science
J. Pept. Sci. 2008; **14**: 1295–1302
Published online 24 October 2008 in Wiley InterScience (www.interscience.wiley.com). DOI: 10.1002/psc.1074

JOURNAL OF PEPTIDE SCIENCE

Second-harmonic generation from Langmuir–Blodgett film of cyclic peptide carrying two disperse red 1 on fused quartz surface

SHIGEKATSU FUJII, TOMOYUKI MORITA and SHUNSASKU KIMURA*

Department of Material Chemistry, Graduate School of Engineering, Kyoto University, Kyoto-Daigaku-Katsura, Nishikyo-ku, Kyoto, Japan

Received 23 May 2008; *Revised 4 August 2008*; *Accepted 7 August 2008*

Abstract: Cyclic octapeptide carrying one or two nonlinear optical chromophores, disperse red 1 (DR-1), was synthesized and immobilized on a substrate to attain an active surface for second-harmonic generation (SHG). Each cyclic octapeptide was transferred on a fused quartz substrate by the Langmuir–Blodgett (LB) method to afford a uniform monolayer. Infrared reflection–absorption spectroscopy of the LB monolayer revealed that the cyclic skeleton lay roughly flat on the surface. The SHG intensity from the monolayer of the cyclic peptide with two DR-1 units was stronger than that from that with one DR-1 unit. The difference is discussed in terms of molecular orientation and surface density of the active chromophores. The cyclic peptide is shown here to be an effective scaffold to modify a substrate surface with functional groups of a monolayer with taking stability of the monolayer and orientation of the functional group into consideration. Copyright © 2008 European Peptide Society and John Wiley & Sons, Ltd.

Keywords: cyclic peptide; scaffold; monolayer; self-assembly; SHG

INTRODUCTION

Recently, various organic second-order nonlinear optical (NLO) materials, which have advantages of their large molecular hyperpolarizability, ultrafast response, and application to various materials, have attracted scientific and technological interest [1–3]. Several methods have been developed for the fabrication to attain noncentrosymmetric molecular single crystals, which generate efficient NLO responses (e.g. second-harmonic generation, SHG) [4–7]. Thin films of NLO materials are also prepared by characteristic methods such as self-assembled monolayers (and multilayers) [8–13], cast or spincoat polymer films treated by poling [14–17], and Langmuir–Blodgett (LB) films [18–22]. The LB method has been successfully applied to amphiphilic chromophores to be immobilized on a wide range of substrates [23–27]. Since the molecules take a specific orientation at the air–water interface, the LB films usually build up macroscopically acentric supramolecular organization on the substrate surface [19–21,28]. However, the LB method sometimes causes technical trouble such as instability and collapse of the monolayer at the air–water interface.

In the ordinary LB method, it is important to choose a proper surface pressure for transfer of the monolayer on subphase, because the molecule by itself can take a free orientation on surface. On the other hand, the use of a tripod- or tetrapod-shaped scaffold is an elegant way to obtain a specific orientation of chromophore on surface [29–32]. In the previous paper, we proposed another method for surface immobilization of using a planar compound as a scaffold [33]. The planar scaffold is easily designed to be attached to surface with a face-to-face contact. This concept will broaden the research area of LB films and can be applied not only to NLO application but to build up other novel and stable LB film materials with various functions.

To point out a further merit of using cyclic peptides as a scaffold, here, we synthesized a novel cyclo[8 + 2DR-1] (Figure 1) carrying two disperse red 1 (DR-1) [34,35] on a scaffold. A few examples of such multichromophoric systems have been reported [36,37]. In our compound, the scaffold may concentrate the chromophore density on surface. Further, two chromophores may cause steric crowding to induce a straight-up orientation of the DR-1 unit on surface, which is favorable for SHG. The two DR-1 units are introduced to the side chains of the tyrosine residues. Prior to LB deposition on substrate surface, the quality of the monolayer at the air–water interface was examined by pressure-area (π-A) isotherms. LB monolayer and second-order NLO property were studied and characterized by UV–vis absorption spectroscopy, Fourier transform infrared reflection–absorption spectroscopy, and SHG measurement.

EXPERIMENTAL

Synthesis of the Cyclic Peptide

Cyclo[8 + 2DR-1] was synthesized according to Scheme 1. The synthesis of cyclo[8 + DR-1] was reported previously [33]. All

*Correspondence to: Shunsasku Kimura, Department of Material Chemistry, Kyoto University, Kyoto-Daigaku-Katsura, Nishikyo-ku, Kyoto 615-8510, Japan; e-mail: shun@scl.kyoto-u.ac.jp

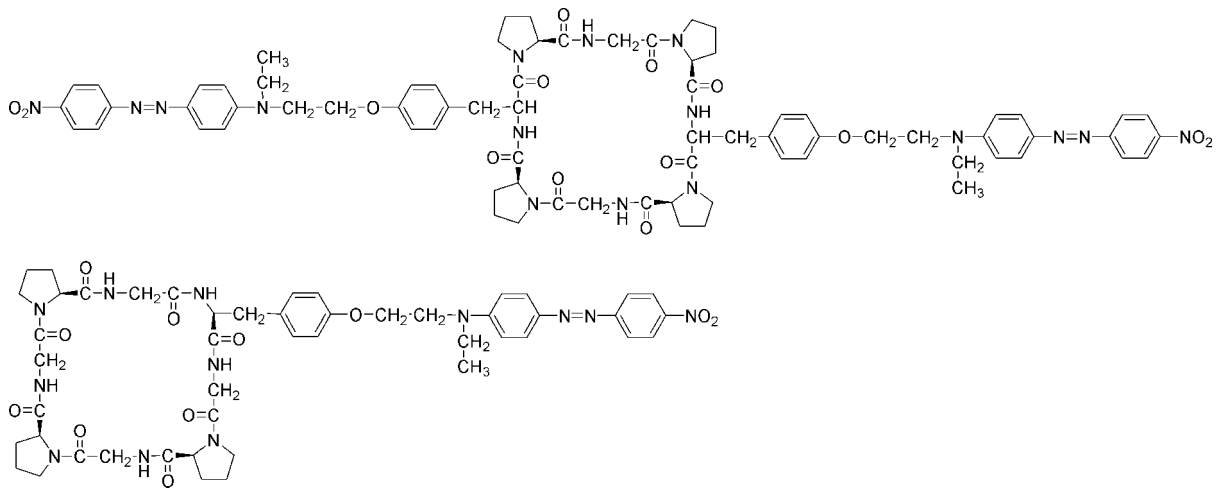

Figure 1 Molecular structures of cyclo[8 + 2DR-1] and cyclo[8 + DR-1].

peptides were synthesized by the conventional liquid-phase method. All intermediates and final products were identified by ^{1}H NMR (400 MHz). The final product was further confirmed by mass spectroscopy.

All reagents and solvents needed for the synthesis were purchased from commercial suppliers and used as received. All NMR spectra were obtained on a Bruker DPX-400 MHz spectrometer, and chemical shifts were given in δ value. Fast atom bombardment mass spectrometry was carried out on a JEOL JMS-HX110A mass spectrometer. Boc-Tyr(DR-1)-OH [38] and Boc-Gly-Pro-OH [39] were synthesized according to the literature.

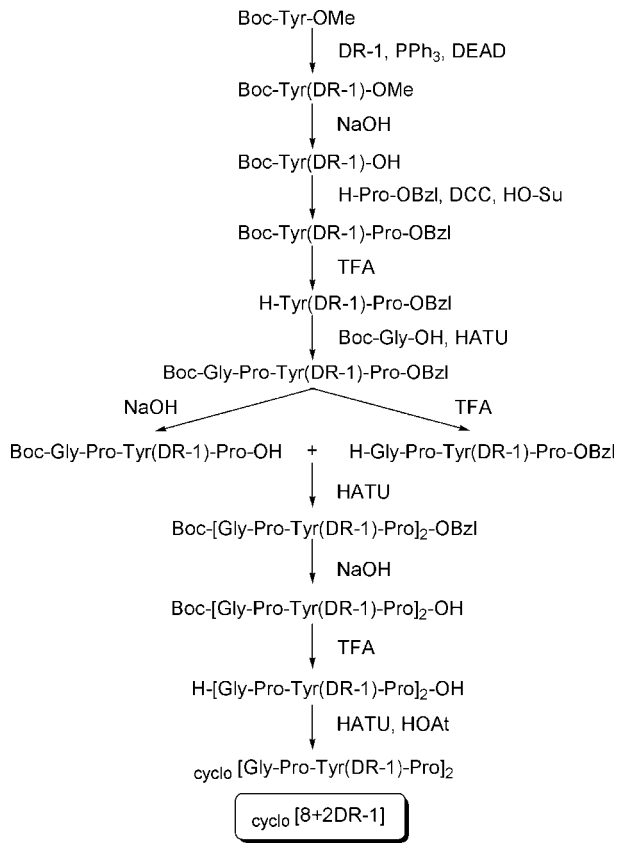

Scheme 1 Synthetic scheme of cyclo[8 + 2DR-1].

B-2(DR-1)-B (Boc-Tyr(DR-1)-Pro-OBzl). Boc-Tyr(DR-1)-OH (4.60 g, 7.96 mmol) and H-Pro-*O*Bzl (1.83 g, 7.59 mmol) in dichloromethane (CH_2Cl_2) was cooled at 0 °C. HOBt (1.08 g, 7.74 mmol), 1-ethyl-3[3-dimethylamino-propyl]carbodiimide hydrochloride (EDC, 1.48 g, 7.74 mmol), and *N*,*N*-diisopropylethylamine (DIEA, 1.32 ml, 7.59 mmol) were successively added, and the solution was stirred at 0 °C for 2 h and at room temperature for overnight. The organic solution was washed successively by water, 4% aqueous sodium bicarbonate ($NaHCO_3$), water, 4% aqueous potassium bisulfate ($KHSO_4$), and water. The organic layer was dried over magnesium sulfate ($MgSO_4$), and concentrated. The residue was purified by a flash chromatography over a silica gel column (first chromatography with eluant of chloroform ($CHCl_3$) followed by $CHCl_3$/methanol (MeOH) = 8/1 v/v, and second chromatography of eluant of $CHCl_3$ followed by $CHCl_3$/diethylether (Et_2O) = 10/1 v/v). Yield: 3.16 g (54.8%).

B-4(DR-1)-B (Boc-Gly-Pro-Tyr(DR-1)-Pro-OBzl). B-2[DR-1]-B was treated with TFA and anisole at 0 °C for 1 h to afford H-2[DR-1]-B. Boc-Gly-Pro-OH (1.03 g, 3.80 mmol) and H-2[DR-1]-B (2.96 g, 3.80 mmol) in CH_2Cl_2 was cooled at 0 °C. HOBt (0.53 g, 3.80 mmol), EDC (0.73 g, 3.80 mmol), and DIEA (1.32 ml, 7.59 mmol) were successively added, and the solution was stirred at 0 °C for 2 h and at room temperature for overnight. The organic solution was successively washed by water, 4% $NaHCO_3$ aqueous solution, water, 4% $KHSO_4$ aqueous solution, and water. The organic layer was dried over $MgSO_4$, and concentrated. The residue was purified by a flash chromatography over a silica gel column (eluant of $CHCl_3/Et_2O = 20/1$ followed by $CHCl_3$/MeOH = 50/1 v/v). The residue was purified by a Sephadex LH-20 column (MeOH as eluant). Yield: 1.83 g (52.3%).

B-8(2DR-1)-B (Boc-(Gly-Pro-Tyr(DR-1)-Pro)$_2$-OBzl). B-4[DR-1]-B was treated with TFA and anisole at 0 °C for 1 h to afford H-4[DR-1]-B. On the other hand, to a solution of B-4[DR-1]-B in a mixture of MeOH and 1,4-dioxane (1/5 v/v) was added a 1 N NaOH aqueous solution. After the solution was stirred at room temperature for 1 h, $CHCl_3$ was added

DOI: 10.1002/psc

to the reaction solution, and the whole solution was washed successively by 4% $KHSO_4$ aqueous solution and water. The organic layer was dried over $MgSO_4$, and concentrated to afford B-4[DR-1]-OH. B-4[DR-1]-OH (355 mg, 0.43 mmol) and H-4[DR-1]-B (400 mg, 0.43 mmol) in *N*,*N*-dimethylformamide (DMF) was cooled at 0 °C. HATU (245 mg, 0.64 mmol) and DIEA (0.24 ml, 1.37 mmol) were successively added, and the solution was stirred at 0 °C for 2 h and at room temperature for overnight. After the solution was condensed, the residue was dissolved in $CHCl_3$ followed by a wash with water. The organic layer was dried over $MgSO_4$, and condensed. The residue was purified by a flash chromatography over a silica gel column (eluant of $CHCl_3$/MeOH = 40/1 followed by $CHCl_3$/MeOH/acetic acid = 25/1/0.2 v/v/v). Yield: 376 mg (53.8%).

Cyclo(8 + 2DR-1) (cyclo(Gly-Pro-Tyr(DR-1)-Pro)$_2$). To a solution of B-8[2DR-1]-B in a mixture of MeOH and 1,4-dioxane (1/2 v/v), 1 N NaOH aqueous solution was added. After the solution was stirred at room temperature for 3 h, $CHCl_3$ was added to the reaction solution, and the solution was washed successively by 4% $KHSO_4$ aqueous solution and water. The organic layer was dried over $MgSO_4$, and concentrated to afford B-8[2DR-1]-OH. B-8[2DR-1]-OH was then treated with TFA and anisole at 0 °C for 1 h to afford H-8[2DR-1]-OH. To a solution of H-8[2DR-1]-OH (106 mg, 0.068 mmol) in DMF, HATU (130 mg, 0.341 mmol) and HOAt (47 mg, 0.341 mmol) were added. A DMF solution containing 0.095 ml DIEA (0.546 mmol) was added in a dropwise way to the reaction solution for 3 h under stirring. Stirring was kept for overnight at room temperature. The solvent was removed by evaporation, and then the residue was purified by a Sephadex LH-20 column (MeOH as eluant). Yield: 38.8 mg (40.0%).

^{1}H NMR (400 MHz, $CDCl_3$): δ (ppm) 1.24 (6H, t, CH_3CH$_2$N), 1.62–2.30 (16H, m, Pro C$_\beta H_2$, C$_\gamma H_2$), 2.70–2.88 (2H, m, Tyr C$_\beta H_2$), 3.17–3.56 (8H, m, Pro C$_\delta H_2$), 3.56 (4H, q, CH$_3$CH_2N), 3.79 (4H, t, NCH_2CH$_2$O), 3.89–4.28 (4H, m, Gly C$_\alpha H_2$), 4.10 (4H, t, NCH$_2$CH_2O), 4.52–4.60 (4H, m, Pro C$_\alpha H$), 4.83 (2H, q, Tyr C$_\alpha H$), 6.76 (8H, d, d, Tyr phenyl-*H*, DR-1 phenyl-*H*), 7.06 (4H, d, Tyr phenyl-*H*), 7.68 (2H, br, Tyr amide N*H*), 7.88 (8H, d, d, DR-1 phenyl-*H*), 7.98 (2H, br, Gly amide N*H*), 8.30 (4H, d, DR-1 phenyl-*H*).

MS (FAB, matrix; nitrobenzylalcohol): *m*/*z* 1421.7 (calcd for $C_{74}H_{85}N_{16}O_{14}$ [(M + H)$^+$] *m*/*z* 1421.64), and *m*/*z* 1443.6 (calcd for $C_{74}H_{84}N_{16}O_{14}Na$ [(M + Na)$^+$] *m*/*z* 1443.63).

π-A Isotherms

Surface pressure-area (π-*A*) isotherms were measured on a film balance (FSD-110, USI Co., Ltd, Japan) with a Langmuir trough (10 cm × 19 cm). Deionized water (resistivity greater than 18 MΩ cm) from a Milli-Q system was used for the aqueous subphase. An aliquot of a chloroform solution of cyclo[8 + 2DR-1] in a concentration range of 0.92–1.4 mM was spread on aqueous subphase using a microsyringe. The monolayer was formed in a gas analogous state and was equilibrated for 15 min prior to compression.

Preparation of LB Films

Two kinds of substrates, gold and fused quartz, were used. The former substrate was prepared by vapor deposition of chromium (30-nm thickness) and gold (200-nm thickness) on a glass substrate. The cyclic peptide monolayer, which was spread on a water subphase, was transferred onto a substrate by the conventional vertical dipping method at a surface pressure of 10 mN/m and a transfer rate of 10 cm^2/min at 25 °C.

Spectroscopy on Films

UV–vis absorption spectra of the films were recorded on a SIMADZU UV-2450. Fourier transform infrared reflection–absorption spectroscopy (FTIR-RAS) spectra were recorded on a Nicolet Magna 850 Fourier transform infrared spectrophotometer and measurements were taken at an incidence angle of 80°. The number of interferogram accumulation was 1000. Geometry of a model cyclic peptide, cyclo(Gly-Pro)$_4$, was optimized to estimate the angles between the ring plane normal and the amide I and II transitions. The initial geometry was generated by a Fujitsu CAChe WorkSystem software (version 6.1.1). The dihedral angles of the peptide backbone were set to be $\omega = 180°$, $\phi = -98°$ and $\psi = 90°$ for the Pro residues, while $\omega = 180°$, $\phi = -175°$, and $\psi = 178°$ for the Gly residues according to the literature [40]. The geometry was then optimized by the Molecular Mechanics program 2 (MM2) method and the semiempirical Austin Model 1 (AM1) method in the MOPAC 2002 package on the same program. The angles between the ring plane normal, and the amide I and II transitions were determined to be 47° and 89°, respectively. The tilt angle of the ring plane normal from the surface normal was determined using an equation, $I_1/I_2 = 1.5\ [(3\cos^2\gamma - 1)\ (3\cos^2\theta_1 - 1) + 2]/[(3\cos^2\gamma - 1)\ (3\cos^2\theta_2 - 1) + 2]$, where I_i, γ, and θ_i ($i = 1$ or 2 corresponding to amide I or amide II) represent the observed absorbance, the tilt angle of the ring plane normal from the surface normal, and the angle between the transition moment and the ring plane normal, respectively.

SHG Measurements

The polarized SHG measurements were carried out on a home-made apparatus in the transmission mode using the 1064-nm light from a Nd : YAG laser (GCR-11, Spectra Physics Inc.) whose pulse width was about 10 ns [41,42]. The experimental setup is shown in Figure 5. The beam area was about 5 mm in diameter. The second-harmonic signal was detected through a monochromator (270M, Spex Inc.) equipped with a photomultiplier (R955, Hamamatsu Photonics Ltd.). The optical setup about the polarization was *p* excitation and *p* detection. The signal from the photomultiplier was accumulated using a digital oscilloscope (54 522A Hewlett Packard Inc.). The sample was rotated on *y*-axis, which is in-plane of the sample surface, from −60° to 60°. The second-harmonic light intensity from a Y-cut quartz with a thickness of 1.046 mm and $d_{11} = 0.34$ pm/V was also measured as reference at the same experimental setup to determine the input light power.

RESULTS AND DISCUSSION

π-A Isotherms

A chloroform solution of cyclo[8 + 2DR-1] was spread on a water subphase to form a stable Langmuir monolayer.

DOI: 10.1002/psc

The Langmuir monolayer was characterized by the measurement of π-A isotherm. The π-A isotherm of the [8 + 2DR-1] monolayer is shown in Figure 2. The monolayer showed a collapse at a pressure of about 30 mN/m, which was much higher than that of cyclo[8 + DR-1] with one DR-1 unit previously reported (17 mN/m). The better film formation of cyclo[8 + 2DR-1] is conceivably due to its C_2 symmetric structure balanced with two bulky chromophores, enabling better molecular packing upon compression. On the other hand, the limiting mean molecular area was about 2.0 nm^2, which was estimated from extrapolating the high-pressure region of the π-A isotherm to zero pressure, while the mean molecular area of cyclo[8 + DR-1] was approximately 1.0 nm^2 [33]. The double value observed for cyclo[8 + 2DR-1] with doubling the number of the DR-1 unit suggests that the DR-1 unit determines the limiting area. This is reasonable because the DR-1 unit is largely tilted in the monolayer as described later in the section of the SHG measurements (more than 45°). Assuming the DR-1 unit as a rod with 0.5 nm diameter and 2.4 nm length and there is no overlap between the chromophores, the molecular area occupied by the DR-1 unit is given approximately by 1.2 nm^2 $\times \sin\gamma_{DR-1}$, where $\sin\gamma_{DR-1}$ is the tilt angle of the DR-1 unit from the surface normal, in case of $\gamma_{DR-1} > 45°$. Using this evaluation method and the tilt angles determined by the SHG measurements discussed later ($\gamma_{DR-1} = 68°$ for cyclo[8 + DR-1] and 49° for cyclo[8 + 2DR-1]), the molecular areas are estimated to be 1.1 and 1.8 nm^2 (0.9 nm^2 $\times$ 2), which are in a good agreement with the experimental values. On the other hand, the area of the cyclic peptide scaffold with a flat orientation on the surface is *ca* 1.5 nm^2 estimated by the molecular modeling described later. The cyclic peptide scaffold is likely to tilt from flat orientation upon compression to match the molecular area in the monolayer with that of the DR-1 unit at least in the cyclo[8 + DR-1] monolayer, whose limiting area (1.0 nm^2) is smaller than the area of the flat peptide scaffold (*ca* 1.5 nm^2). Each monolayer was transferred on a substrate by the vertical dipping method at a surface pressure of 10 mN/m, where the molecular areas were 0.8 nm^2 for cyclo[8 + DR-1] and 1.8 nm^2 for cyclo[8 + 2DR-1], respectively.

IR-RAS

Molecular orientation of the peptide scaffold in the cyclo[8 + 2DR-1] monolayer prepared on gold was studied by IR-RAS. In IR-RAS, the transition dipole moments which are normal to the surface are selectively excited, and those which are parallel to the surface are essentially inactive [43]. Amide I band is derived primarily from peptide C=O stretching, and amide II band is a combination of mainly NH in-plane bending and CN stretching [44]. The IR-RAS spectra of the

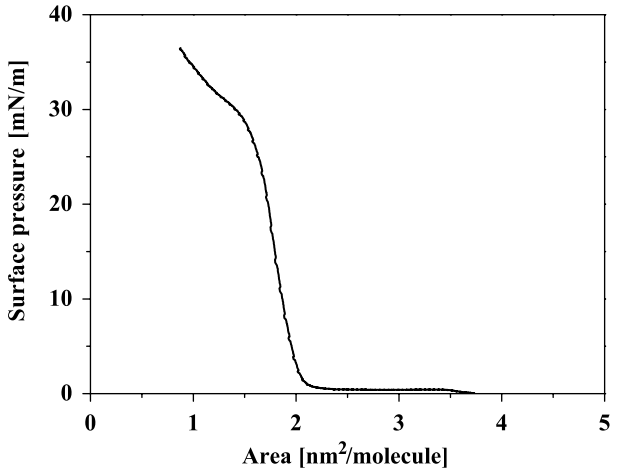

Figure 2 π-A isotherm of cyclo[8 + 2DR-1].

cyclo[8 + 2DR-1] LB monolayer on gold and in bulk are shown in Figure 3. The amide I and II bands are seen at 1650 and 1550 cm^{-1}, respectively. The absorbance ratios of the amide I and II are 3.0 for the monolayer while 1.9 for the bulk. From the absorbance ratios, the tilt angles of the ring plane normal from the surface normal can be determined. The geometry of a model cyclic peptide, cyclo(Gly–Pro)$_4$, was optimized by the MM2 and AM1 methods using its dihedral angles reported in the literature, and the angles between the ring plane normal, and the amide I and II transitions were estimated to be 47° and 89°, respectively. Using these angles, the tilt angle of cyclo[8 + 2DR-1] was determined to be 39° for the LB monolayer. For the bulk peptide, the angle was calculated apparently to be 48°, which is agreeable with a random orientation in bulk, 54°. The smaller tilt angle in the LB monolayer indicates that the orientation of the peptide cyclic skeleton is closer to a parallel orientation to the surface. In the optimized geometry of cyclo(Gly–Pro)$_4$, there are four in-plane equatorial C=O groups and four out-plane axial C=O groups. All the latter groups are unidirectional and their oxygen atoms protrude over the same side of the ring plane. It is thus suspected that this side acts as a hydrophilic side of the ring and it should facilitate parallel orientation of the peptide ring on water.

UV–visible Absorption

The UV–vis transmission spectra at the normal incidence of cyclo[8 + 2DR-1] and cyclo[8 + DR-1] in the LB monolayers prepared on fused quartz are shown in Figure 4. The absorption maxima of cyclo[8 + 2DR-1] (peak position at 471 nm) is slightly red-shifted with respect to that of cyclo[8 + DR-1] (peak position at 465 nm). The slight shift of cyclo[8 + 2DR-1] can be the result of interactions among the neighboring DR-1 units. The DR-1 unit is largely tilted in the cyclo[8 + DR-1] monolayer. On the other hand, in the cyclo[8 + 2DR-1] monolayer, the two chromophores

DOI: 10.1002/psc

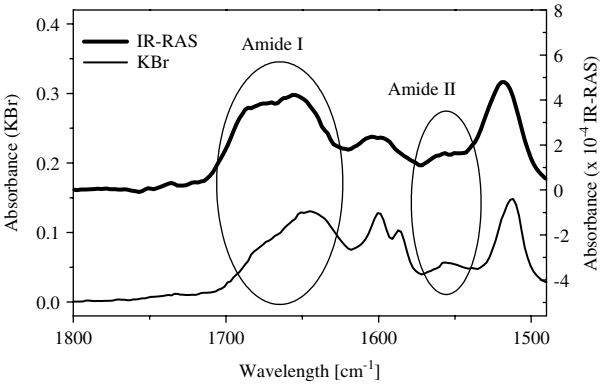

Figure 3 IR spectra of cyclo[8 + 2DR-1] on gold and in a KBr pellet.

are tethered to one scaffold to obtain more vertically orientation of the DR-1 units. Therefore, interactions among the chromophores should be strong enough in the cyclo[8 + 2DR-1] monolayer to cause a shift in the absorption [45]. For example, a head-to-tail arrangement of the DR-1 units in tilt orientation should cause a red-shift as seen in a *J*-aggregate. It is rather surprising that the absorption intensities were nearly the same for both monolayers. Since the transition moment of this absorption is along the molecular axis of the DR-1 unit, its absorbance should show a tilt-angle dependence in the form of $\sin^2 \gamma_{DR-1}$. The surface densities of the chromophore are 1/0.8 nm^{-2} for cyclo[8 + DR-1] and 2/1.8 nm^{-2} for cyclo[8 + 2DR-1], from the molecular area at the monolayer transfer. Thus, there should be $(1/0.8)\sin^2 68^\circ$:$(2/1.8)\sin^2 49^\circ$ (1.7 : 1) absorbance difference between the cyclo[8 + DR-1] and cyclo[8 + 2DR-1] monolayers. The reason for this disagreement is yet to be clear, but one possibility is that the strong interchromophoric interaction occurring in the cyclo[8 + 2DR-1] monolayer increases the absorptivity as well, leading to the same absorbance by chance.

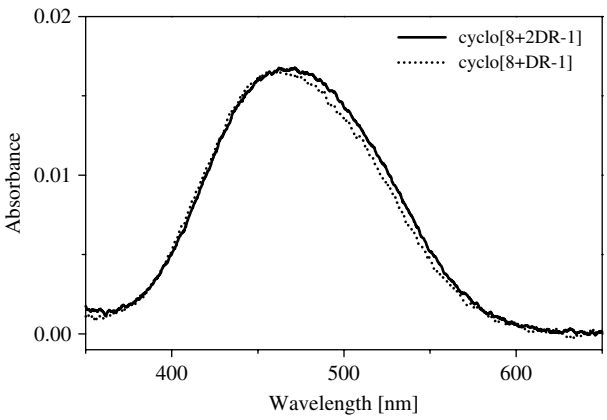

Figure 4 UV–vis spectra of cyclo[8 + 2DR-1] (solid line) and cyclo[8 + DR-1] (dotted line) LB monolayers on fused quartz.

SHG Measurements

SHG measurements were carried out on the LB monolayers prepared on fused quartz to determine nonlinear susceptibilities and the orientation of the DR-1 unit. A *p*-polarized 1064 nm light was introduced to the LB monolayer-covered substrate and the *p*-polarized 532 nm second-harmonic signal transmitted through the sample was detected at various incident angles. The intensity of the second-harmonic signal from Y-cut quartz measured at the same experimental setup was used as reference. The results are shown in Figure 5. A characteristic fringe pattern depending on the incident angles by the interference between the signals generated from the monolayers on both sides of the substrate was clearly observed [46–48]. The fringe minima of nearly zero indicates the uniformity of the LB monolayers [49]. The results are analyzed under assumptions that the molecular hyperpolarizability is dominant in the direction of the DR-1 long axis and the chromophores are uniaxially distributed with a certain tilt angle from the surface normal (γ_{DR-1}). In this case, three components of nonlinear susceptibilities (χ_{xxz}, χ_{zxx}, and χ_{zzz}) are non-zero. The second-harmonic signal ($I_{pp}{}^{2\omega}$) is given by the following theoretical expression for molecular layers on one side of the substrate developed by Katz *et al.* [8] with a small modification,

$$
\begin{aligned}
I_{pp}^{2\omega} &= C(\theta)|(2\chi_{xxz} + \chi_{zxx})\cos^2\theta_f + \chi_{zzz}\sin^2\theta_f|^2 \\
C(\theta) &= \left[\frac{\pi}{2}\frac{l_f}{l_{quartz}}\right]^2\left[\frac{n_{quartz}}{n_f}\right]^3\frac{I_{quartz}{}^{2\omega}}{|\chi_{quartz}|^2}[T_p^{a\to f}(\theta)]^2 T_p^{f\to s} \\
&\quad (\theta)T_p^{s\to a}(\theta)\frac{\sin^2\theta_f\cos\theta}{\cos^3\theta_f} \\
d_{xxz} &= d_{zxx} = \frac{1}{2}N_s\beta\cos\gamma_{DR-1}\sin^2\gamma_{DR-1}f(2\omega)f(\omega)^2 \\
d_{zzz} &= N_s\beta\cos^3\gamma_{DR-1}f(2\omega)f(\omega)^2 \\
f(\omega) &= \frac{n_f(\omega)^2 + 2}{3}
\end{aligned}
\qquad (1)
$$

where θ is the incident angle, θ_f the angle of refraction in the film, l_f the number of monolayers, l_{quartz} the coherence length of Y-cut quartz, n_i the refractive index of i (f; film), $I_{quartz}{}^{2\omega}$ the second-harmonic intensity from Y-cut quartz at the first maximum from normal incidence, χ_{quartz} the nonlinear susceptibility of Y-cut quartz ($\chi_{xxx} = 0.68$ pm/V $= 1.6 \times 10^{-9}$ cm^2/esu), $T_p{}^{i\to j}(\theta)$ the transmittance for *p*-polarized light of the interface from phase *i* to phase j (a: air, f: film, s: substrate), N_s the surface density of the DR-1 unit in the monolayer, β the hyperpolarizability of DR-1 along its long axis, γ_{DR-1} the tilt angle of the DR-1 unit from the surface normal, and $f(2\omega)$ and $f(\omega)$ the Lorentz factors to correct local field effect in the film for the fundamental and second-harmonic waves. It should be noted that this formula was developed for the molecular layers deposited on one side of a substrate

DOI: 10.1002/psc

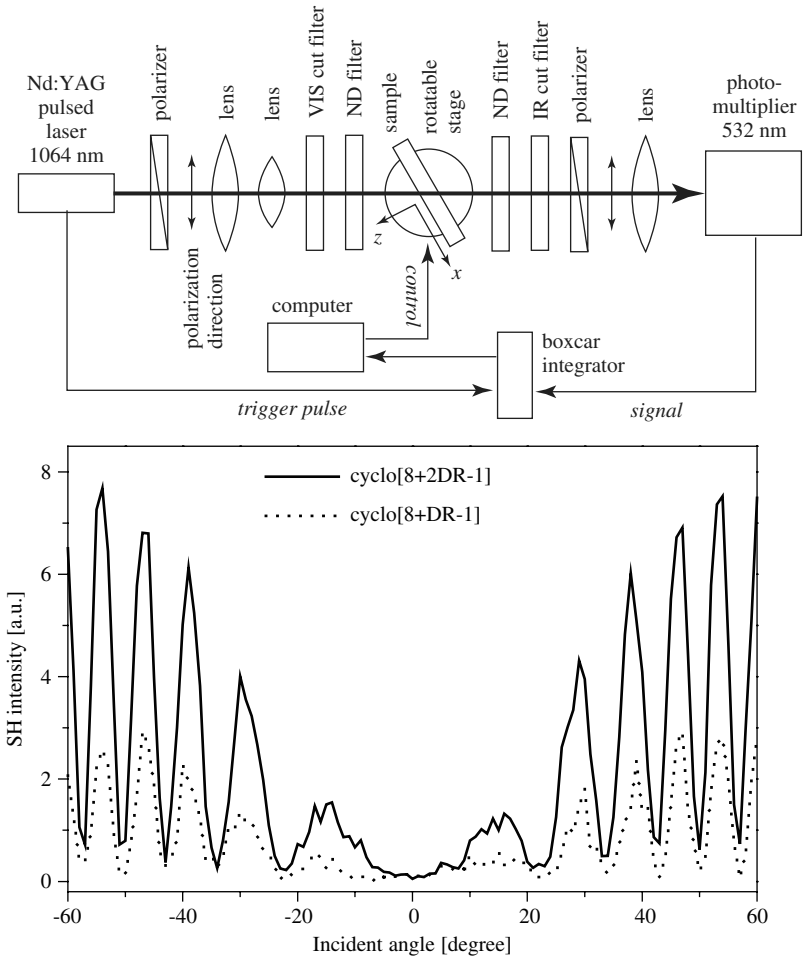

Figure 5 Experimental setup for SHG measurements (top), the second-harmonic signals from the monolayers of cyclo[8 + 2DR-1] (solid line), and cyclo[8 + DR-1] (dotted line) on fused quartz (bottom).

and the interference from monolayers deposited on both sides of a substrate was not considered. Therefore, the experimental data were fitted at the fringe peak tops with the number of the monolayers being 2.

The fitting of the experimental data gave γ_{DR-1} of 68° for cyclo[8 + DR-1] and 49° for cyclo[8 + 2DR-1], respectively, as mentioned earlier. As indicated by the smaller tilt angle, the monolayer regularity is higher in cyclo[8 + 2DR-1] monolayer which is in line with the π-*A* isotherm observation. The DR-1 surface densities were determined to be 0.9×10^{14} molecules/cm^2 for cyclo[8 + DR-1] and 1.1×10^{14} molecules/cm^2 for cyclo[8 + 2DR-1], respectively. The former density is 30% less than the calculated density on the basis of the molecular area at the monolayer transfer (1.25×10^{14} molecules/cm^2), whereas the latter value agrees well with the calculated density (1.1×10^{14} molecules/cm^2). This finding suggests that some portion of the DR-1 units may have antiparallel arrangement with the neighbors to loose the NLO activity in the cyclo[8 + DR-1] monolayer where the structural regularity is low due to the large tilt angle. On the other hand, β was 65×10^{-30} cm^5/esu which is close to the reported value in the literature [50] (*ca* 45×10^{-30} cm^5/esu). The nonlinear susceptibilities were $\chi_{xxz} = \chi_{zxx} = 5.4$ pm/V and $\chi_{zzz} = 1.8$ pm/V for the cyclo[8 + DR-1] monolayer and $\chi_{xxz} = \chi_{zxx} = 7.9$ pm/V and $\chi_{zzz} = 12.0$ pm/V for the cyclo[8 + 2DR-1] monolayer, respectively. Taken together, the present method to incorporate two DR-1 units into the cyclic peptide scaffold is a good way to make the substrate surface SHG active with using the LB technique on the surface modification. Further, the second-harmonic signal intensity from the cyclic peptide monolayer has kept constant for several months at room temperature, indicating the good stability of the orientation of the DR-1 units on the surface with the cyclic peptide scaffold.

CONCLUSION

We have shown the availability of the cyclic octapeptide as a scaffold for vertical orientation of two nonlinear-optically active DR-1 units. The DR-1 tethered peptide formed a stable Langmuir monolayer at the air–water interface, and the formed monolayer was successfully transferred onto a substrate surface. The LB films

DOI: 10.1002/psc

generated a 532-nm second-harmonic signal upon irradiation of a 1064-nm light. The intensity of the second-harmonic signal was successfully explained on the basis of the molecular orientation, surface density, and hyperpolarizability of the DR-1 unit. More stable and regular monolayer structure, more vertical orientation, and noncentrosymmetric arrangement of the DR-1 unit, and accordingly the better SHG performance, were demonstrated in the present system, two DR-1 units on the cyclic peptide, compared with the reference system composed of the cyclic peptide with one DR-1 unit. The balanced chemical structure composed of a cyclic peptide scaffold and two bulky chromophores should be the reason for those superiorities. Cyclic peptides can be therefore one of useful scaffolds for immobilization of various functional groups on surface.

Acknowledgements

The authors appreciate Prof. K. Hirao, Prof. K. Tanaka, and Mr K. Higashi (Graduate School of Engineering, Kyoto University, Japan) for their help in the SHG measurements.

REFERENCES

1. Dalton LR, Harper AW, Ghosn R, Steier WH, Ziari M, Fetterman H, Shi Y, Mustacich RV, Jen AKY, Shea KJ. Synthesis and processing of improved organic 2nd-order nonlinear-optical materials for applications in photonics. *Chem. Mater.* 1995; **7**: 1060–1081.
2. Marder SR, Kippelen B, Jen AKY, Peyghambarian N. Design and synthesis of chromophores and polymers for electro-optic and photorefractive applications. *Nature.* 1997; **388**: 845–851.
3. Verbiest T, Houbrechts S, Kauranen M, Clays K, Persoons A. Second-order nonlinear optical materials: recent advances in chromophore design. *J. Mater. Chem.* 1997; **7**: 2175–2189.
4. Evans OR, Lin WB. Crystal engineering of NLO materials based on metal-organic coordination networks. *Acc. Chem. Res.* 2002; **35**: 511–522.
5. Marder SR, Perry JW, Yakymyshyn CP. Organic salts with large 2nd-order optical nonlinearities. *Chem. Mater.* 1994; **6**: 1137–1147.
6. Levine BF, Bethea CG, Thurmond CD, Lynch RT, Bernstein JL. Organic-crystal with an exceptionally large optical 2nd-harmonic coefficient - 2-methyl-4-nitroaniline. *J. Appl. Phys.* 1979; **50**: 2523–2527.
7. Oudar JL, Hierle R. Efficient organic crystal for nonlinear optics - methyl-(2,4-dinitrophenyl)-aminopropanoate. *J. Appl. Phys.* 1977; **48**: 2699–2704.
8. Katz HE, Scheller G, Putvinski TM, Schilling ML, Wilson WL, Chidsey CED. Polar orientation of dyes in robust multilayers by zirconium phosphate-phosphonate interlayers. *Science* 1991; **254**: 1485–1487.
9. Dhirani A, Lin PH, GuyotSionnest P, Zehner RW, Sita LR. Self-assembled molecular rectifiers. *J. Chem. Phys.* 1997; **106**: 5249–5253.
10. Li DQ, Swanson BI, Robinson JM, Hoffbauer MA. Porphyrin based self-assembled monolayer thin-films - synthesis and characterization. *J. Am. Chem. Soc.* 1993; **115**: 6975–6980.
11. Moon JH, Kim JH, Kim K, Kang TH, Kim B, Kim CH, Hahn JH, Park JW. Absolute surface density of the amine group of the aminosilylated thin layers: Ultraviolet-visible spectroscopy, second harmonic generation, and synchrotron-radiation photoelectron spectroscopy study. *Langmuir* 1997; **13**: 4305–4310.
12. Heflin JR, Figura C, Marciu D, Liu Y, Claus RO. Thickness dependence of second-harmonic generation in thin films fabricated from ionically self-assembled monolayers. *Appl. Phys. Lett.* 1999; **74**: 495–497.
13. Roscoe SB, Kakkar AK, Marks TJ, Malik A, Durbin MK, Lin WP, Wong GK, Dutta P. Self-assembled chromophoric NLO-active monolayers. X-ray reflectivity and second-harmonic generation as complementary probes of building block-film microstructure relationships. *Langmuir* 1996; **12**: 4218–4223.
14. Bauer S. Poled polymers for sensors and photonic applications. *J. Appl. Phys.* 1996; **80**: 5531–5558.
15. Kajzar F, Lee KS, Jen AKY. Polymeric materials and their orientation techniques for second-order nonlinear optics. *Polymers For Photonics Applications Ii* 2003; **161**: 1–85.
16. Hayden LM, Sauter GF, Ore FR, Pasillas PL, Hoover JM, Lindsay GA, Henry RA. 2nd-order nonlinear optical measurements in guest-host and side-chain polymers. *J. Appl. Phys.* 1990; **68**: 456–465.
17. Singer KD, Kuzyk MG, Holland WR, Sohn JE, Lalama SJ, Comizzoli RB, Katz HE, Schilling ML. Electro-optic phase modulation and optical 2nd-harmonic generation in corona-poled polymer-films. *Appl. Phys. Lett.* 1988; **53**: 1800–1802.
18. Ashwell GJ, Hargreaves RC, Baldwin CE, Bahra GS, Brown CR. Improved 2nd-harmonic generation from Langmuir-Blodgett-films of hemicyanine dyes. *Nature* 1992; **357**: 393–395.
19. Carpenter MA, Willand CS, Penner TL, Williams DJ, Mukamel S. Aggregation in hemicyanine dye Langmuir-Blodgett-films - ultraviolet visible absorption and 2nd harmonic-generation studies. *J. Phys. Chem.* 1992; **96**: 2801–2804.
20. Liu YQ, Xu Y, Zhu DB, Wada T, Sasabe H, Zhao XS, Xie XM. Optical 2nd-harmonic generation from Langmuir-Blodgett-films of an asymmetrically substituted phthalocyanine. *J. Phys. Chem.* 1995; **99**: 6957–6960.
21. Wijekoon W, Wijaya SK, Bhawalkar JD, Prasad PN, Penner TL, Armstrong NJ, Ezenyilimba MC, Williams DJ. Second harmonic generation in multilayer Langmuir-Blodgett films of blue transparent organic polymers. *J. Am. Chem. Soc.* 1996; **118**: 4480–4483.
22. Umemura Y, Yamagishi A, Schoonheydt R, Persoons A, De Schryver F. Langmuir-Blodgett films of a clay mineral and ruthenium(II) complexes with a noncentrosymmetric structure. *J. Am. Chem. Soc.* 2002; **124**: 992–997.
23. Blodgett KB. Films built by depositing successive monomolecular layers on a solid surface. *J. Am. Chem. Soc.* 1935; **57**: 1007–1022.
24. Blodgett KB, Langmuir I. Built-up films of barium stearate and their optical properties. *Physical Review* 1937; **51**: 964–982.
25. Roberts GG. An Applied Science Perspective Of Langmuir-Blodgett Films. *Advances In Physics* 1985; **34**: 475–512.
26. Zasadzinski JA, Viswanathan R, Madsen L, Garnaes J, Schwartz DK. Langmuir-Blodgett-Films. *Science* 1994; **263**: 1726–1733.
27. Meyer E, Howald L, Overney RM, Heinzelmann H, Frommer J, Guntherodt HJ, Wagner T, Schier H, Roth S. Molecular-resolution images of Langmuir-Blodgett-films using atomic force microscopy. *Nature* 1991; **349**: 398–400.
28. Ashwell GJ. Langmuir-Blodgett films: molecular engineering of non-centrosymmetric structures for second-order nonlinear optical applications. *J. Mater. Chem.* 1999; **9**: 1991–2003.
29. Zhu LH, Tang HQ, Harima Y, Yamashita K, Hirayama D, Aso Y, Otsubo T. Electrochemical properties of self-assembled monolayers of tripod-shaped molecules and their applications to organic light-emitting diodes. *Chem. Commun.* 2001; 1830–1831.
30. Zhu LH, Tang HQ, Harima Y, Yamashita K, Aso Y, Otsubo T. Enhanced hole injection in organic light-emitting diodes consisting of self-assembled monolayer of tripod-shaped pi-conjugated thiols. *J. Mater. Chem.* 2002; **12**: 2250–2254.

31. Deng XB, Mayeux A, Cai CZ. An efficient convergent synthesis of novel anisotropic adsorbates based on nanometer-sized and tripod-shaped oligophenylenes end-capped with triallylsilyl groups. *J. Org. Chem.* 2002; **67**: 5279–5283.
32. Kopaczynska M, Wang TY, Schulz A, Dudic M, Casnati A, Sansone F, Ungaro R, Fuhrhop JH. Scanning force microscopy of upright-standing, isolated calixarene-porphyrin heterodimers. *Langmuir* 2005; **21**: 8460–8465.
33. Fujii S, Morita T, Umemura J, Kimura S. Cyclic peptides as scaffold for oriented functional groups on surface. *Thin Solid Films* 2006; **503**: 224–229.
34. Taunaumang H, Herman, Tjia MO, Samoc M. Electric field induced second harmonic generation in vacuum evaporated Disperse Red 1 films. *Optical Materials* 2003; **22**: 289–294.
35. Sekkat Z, Dumont M. Photoassisted poling of azo dye doped polymeric films at room-temperature. *Applied Physics B-Photophysics And Laser Chemistry* 1992; **54**: 486–489.
36. Kauranen M, Verbiest T, Boutton C, Teerenstra MN, Clays K, Schouten AJ, Nolte RJM, Persoons A. Supramolecular 2nd-order nonlinearity of polymers with orientationally correlated chromophores. *Science* 1995; **270**: 966–969.
37. Kenis PJA, Noordman OFJ, Houbrechts S, van Hummel GJ, Harkema S, van Veggel F, Clays K, Engbersen JFJ, Persoons A, van Hulst NF, Reinhoudt DN. Second-order nonlinear optical properties of the four tetranitrotetrapropoxycalix[4]arene conformers. *J. Am. Chem. Soc.* 1998; **120**: 7875–7883.
38. Wennemers H, Conza M, Nold M, Krattiger P. Diketopiperazine receptors: A novel class of highly selective receptors for binding small peptides. *Chem.-A Euro. J.* 2001; **7**: 3342–3347.
39. Deber CM, Blout ER. Cyclic Peptides.7. Synthesis and characterization of cyclic peptides with repeating Pro-Gly sequences. *Isr. J. Chem.* 1974; **12**: 15–29.
40. Madison V, Deber CM, Blout ER. Cyclic Peptides.17. Metal and amino-acid complexes of cyclo(Pro-Gly)4 and analogs studies by nuclear magnetic-resonance and circular-dichroism. *J. Am. Chem. Soc.* 1977; **99**: 4788–4798.
41. Tanaka K, Narazaki A, Hirao K, Soga N. Optical second harmonic generation in poled MgO-ZnO-TeO_2 and B2O3-TeO_2 glasses. *J. Non-Cryst. Solids* 1996; **203**: 49–54.
42. Narazaki A, Tanaka K, Hirao K. Optical second-order nonlinearity of transparent glass-ceramics containing $BaTiO_3$ precipitated via surface crystallization. *J. Mater. Res.* 1999; **14**: 3640–3646.
43. Umemura J, Kamata T, Kawai T, Takenaka T. Quantitative-evaluation of molecular-orientation in thin Langmuir-Blodgett films by FT-IR transmission and reflection absorption-spectroscopy. *J. Phys. Chem.* 1990; **94**: 62–67.
44. Kim HS, Hartgerink JD, Ghadiri MR. Oriented self-assembly of cyclic peptide nanotubes in lipid membranes. *J. Am. Chem. Soc.* 1998; **120**: 4417–4424.
45. Mishra A, Behera RK, Behera PK, Mishra BK, Behera GB. Cyanines during the 1990s: A review. *Chem. Rev.* 2000; **100**: 1973–2011.
46. Yitzchaik S, Marks TJ. Chromophoric self-assembled superlattices. *Acc. Chem. Res.* 1996; **29**: 197–202.
47. Johal MS, Parikh AN, Lee Y, Casson JL, Foster L, Swanson BI, McBranch DW, Li DQ, Robinson JM. Study of the conformational structure and cluster formation in a Langmuir-Blodgett film using second harmonic generation, second harmonic microscopy, and FTIR spectroscopy. *Langmuir* 1999; **15**: 1275–1282.
48. Shimazaki Y, Ito S, Tsutsumi N. Adsorption-induced second harmonic generation from the layer-by-layer deposited ultrathin film based on the charge-transfer interaction. *Langmuir* 2000; **16**: 9478–9482.
49. Casson JL, Wang HL, Roberts JB, Parikh AN, Robinson JM, Johal MS. Kinetics and interpenetration of ionically self-assembled dendrimer and PAZO multilayers. *J. Phys. Chem. B* 2002; **106**: 1697–1702.
50. Ekhoff JA, Westerbuhr SG, Rowlen KL. Evidence of spontaneous multilayer formation for Disperse Red-1 at a fused-silica/2-propanol interface. *Langmuir* 2001; **17**: 7079–7084.

DOI: 10.1002/psc